Can WAAS Availability Be Inferred From Geomagnetic Data? An Analysis

Seebany Datta-Barua, Todd Walter, Juan Blanch, Per Enge
Stanford University

Abstract

The Federal Aviation Administration's Wide Area Augmentation System (WAAS) provides high integrity GPS-based precision navigation service to users in the conterminous United States (CONUS). User integrity is ensured by bounding all possible GPS error sources, of which the ionospheric delay is the largest and most variable. In particular, during severe ionospheric storms, the WAAS Irregularity Detector alerts that the errors cannot be bounded tightly enough to allow for precision navigation service, and protects users in real-time by lowering precision navigation service availability.

As a result, a question of interest often arises: can we know in advance that WAAS availability will be reduced and if so, what are the reliable indicators? A current heuristic method based on observed magnetosphere-ionosphere coupling is to be on alert when the planetary index of geomagnetic activity Kp reaches the higher range of its possible values. However, the Kp index is anecdotally known to have a high false alarm rate for WAAS availability. Kp has been known to reach its highest value on days for which there has been a negligible decrease in WAAS precision service availability.

This paper is an exploration of how Kp and Dst perform as indicators of WAAS LPV service availability. We examine this question by computing the correlation between the WAAS Irregularity Detector's chi-squared values, representing WAAS availability, for the known WAAS storm (i.e. low-availability) days and the geomagnetic indices of Kp and Dst. We show that Kp shows moderate correlation with the observation of WAAS-effective storms, and that Dst has a strong negative correlation with the log of the chi-squared ratio. We find that Kp also yields a higher false alarm rate than Dst. This work provides preliminary evidence that Dst is slightly more indicative of WAAS availability than Kp.

Introduction

The Wide Area Augmentation System (WAAS) was commissioned by the Federal Aviation Administration (FAA) in July of 2003. Its function is to provide high accuracy, high integrity navigation service to aircraft operating within the conterminous U.S. (CONUS). The WAAS network consists of 25 Reference Stations (WRS), each of which has three colocated dual frequency GPS receivers, two Master Stations (WMS), and two Inmarsat geostationary satellites which broadcast the corrections to users in CONUS who have WAAS-enabled GPS receivers. The primary function of WAAS is not only to provide error corrections to users' GPS measurements, but also to provide confidence bounds on those corrections. Integrity is an assurance on how near the estimate the true position can be guaranteed to be with an extremely high degree of confidence.

WAAS provides several levels of service for navigation both en route and landing, of which the most stringent integrity is required for precision approach to a runway and is known as LPV (Lateral Precision with Vertical guidance). Availability is defined as how often a user is receiving this high-integrity level of service. Coverage measures what percentage of CONUS is achieving a specified level of availability. Since coverage is effectively a measure of availability, such that low coverage tends to imply low availability and vice versa, in this paper the words "coverage" and "availability" are often used interchangeably.

One of the primary factors that reduces WAAS LPV service availability is disturbed ionospheric conditions. WAAS broadcasts estimates of the vertical ionospheric delay over CONUS by treating the ionosphere as a thin shell at 350 km altitude and performing a planar fit at each point in 5x5 degree grid above CONUS, based on the nearest measurements to that Ionospheric Grid Point (IGP). As part of integrity assurance the WAAS algorithm includes an Irregularity Detector. For each planar fit performed at each IGP, the chi-squared statistical consistency value χ^2 is computed. If χ^2 exceeds a threshold, the measurements are inconsistent with a planar model. During these periods the protection factor is set to a value too high to support vertical guidance. The result is that the price of maintaining high integrity even during ionospheric storms is low availability for affected users.

Motivation

Figure 1 shows in solid red line the percentage of the country that was offered LPV service at least 95% of the day for each day from July 1, 2003, through March 1, 2005 [Refs 1-5]. The maximum value of Kp, a worldwide average index of geomagnetic activity, is multiplied by a factor of ten for greater visibility and plotted with blue dots for the same period of time. Kp ranges in thirds from 0 to 9. Geomagnetic activity – which includes not only the core field of the earth, but also fields produced by currents in the upper atmosphere and magnetosphere – is high when Kp takes on its larger values, e.g. 7, 8, 9. Low geomagnetic activity is characterized by low Kp values, 0, 1, 2. The most striking feature of Figure 1 is that while

on the whole LPV is available at least 95% of the time for 95% or more of the country, the coverage (red) drops drastically when Kp reaches its highest values.

This is a tantalizing clue. It indicates that we should be able to have some idea, at best during and at worst after the fact, of which days have low availability based on ionospheric activity. Ideally, simply by looking at some geomagnetic index or another, we would like to be able to know which days in the past warrant further study, from a WAAS operational standpoint.

However, Kp may not be the best predictor of low-availability days. Notice that there are days for which the maximum Kp that day reached 7 or even 7.3 with negligible effect on coverage (e.g. day 50) and there are also days for which a Kp of only 6.3 reduced coverage to less than 50% (day 280). These false alarms and missed detections of low-availability may be due in part to the nature of the Kp index. It is a composite index based on activity measured at several mid-latitude stations primarily in the northern hemisphere worldwide, each of whose individual score is based roughly on the logarithm of the greatest variation in locally measured B field over a three-hour period, but is adjusted to that location. Because it is a global measure and because it is reported only once every three hours, it may not provide the best spatial and temporal resolution to indicate ionospheric behavior over CONUS alone over few-hour time scales.

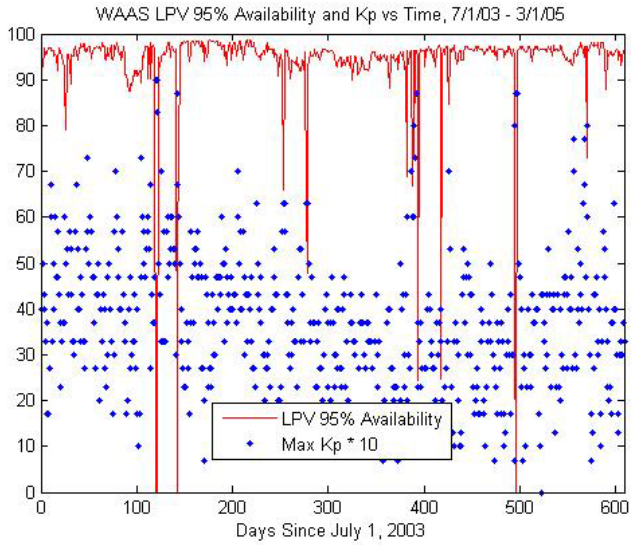

Figure 1: WAAS LPV 95% service coverage and daily maximum Kp x 10 from July 1, 2003, through March 1, 2005.

For better temporal resolution we turn to another measure of geomagnetic activity known as Dst (Disturbance, storm-time), the hourly measure of ring current activity worldwide. Figure 2 shows the same LPV 95% coverage curve as a solid red line as Figure 1. The blue dotted line shows the most extreme Dst measurements on each day. The plot shows that Dst has similar detection properties for the worst storms; major losses of availability occurred when Dst was extremely negative (in the -100s of nT). From these plots though it is not clear whether a Dst threshold can be chosen that will yield a lower number of false alarms than Kp. This paper will examine that issue.

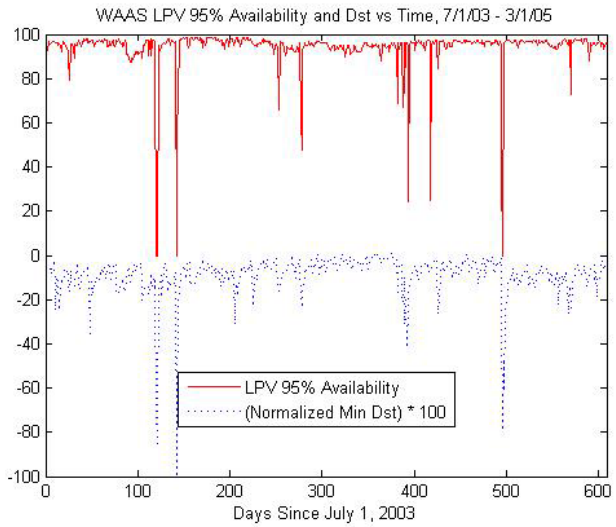

Figure 2: WAAS LPV 95% Service Coverage and Daily Minimum Dst (normalized to -1 and multiplied by 100) from July 1, 2003, through March 1, 2005.

Measuring Availability through Chi^2

Although availability is what we would like to be able to predict, the 95% coverage percentage plotted in solid red in Figure 1 and Figure 2 has advantages and disadvantages. WAAS availability is not always lost exclusively because of ionospheric activity. The two days of 25% LPV availability shown both in Figure 1 and Figure 2 just before and after day 400 were reported to be due to a transmission outage of several hours at one of the WAAS GEOs [5]. Also, the simplicity of the 95% coverage percentage in being a single daily number washes out any detailed spatial and temporal information. Overall CONUS coverage is averaged over each of the IGPs, each of whose individual availability is determined by the WAAS Ionospheric Irregularity Detector. Therefore, to obtain more specific availability information and to ascertain that the availability loss is due to the ionosphere, we use historical WAAS data sets to compute χ^2 as the Irregularity Detector would have done in real-time, and use it as a surrogate for availability.

The WAAS data sets are post-processed collections, known as "supertruth," of the ionospheric measurements made at each of the 25 WRSs.

Table 1

Set No.	Date(s)	Availability Measure	Percent Coverage
1	Jan 11, 2000	Chi^2 (Fig 4)	Expected low
2	Jan 22, 2000	Chi^2 (Fig 4)	Expected low
3	Feb 12, 2000	Chi^2 (Fig 4)	Expected low
4	Mar 26-27, 2000	Chi^2 (Fig 4)	Expected high
5	Apr 5-8, 2000	Chi^2 (Fig 4)	Expected to be 0, Apr 6-8
6	Apr 24, 2000	Chi^2 (Fig 4)	Expected high
7	May 24-25, 2000	Chi^2 (Fig 4)	Expected high
8	Jun 6-8, 2000	Chi^2 (Fig 4)	Expected high
9	Jul 2, 2000	Chi^2 (Fig 4)	Expected high
10	Jul 15-16, 2000	Chi^2 (Fig 4)	Expected to be 0
11	Aug 11-12, 2000	Chi^2 (Fig 4)	Expected low, Aug 11
12	Nov 29, 2000	Chi^2 (Fig 4)	Expected low
13	Mar 20, 2001	Chi^2 (Fig 4)	Expected low
14	Mar 31-April 1, 2001	Chi^2 (Fig 4)	Expected low
15	Apr 11, 2001	Chi^2 (Fig 4)	Expected low
16	Oct 3, 2001	LNAV/VNAV 95%	60% pre-GIVE monitor, (expect 95% post)
17	Oct 21-22, 2001	LNAV/VNAV 95%	15,25% pre-GIVE monitor, (expect 50,60% post)
18	Nov 6, 2001	Chi^2 (Fig 4)	Expected low
19	Nov 24, 2001	Chi^2 (Fig 4)	Expected low
20	Apr 18, 2002	LNAV/VNAV 95%	79
21	Apr 20, 2002	LNAV/VNAV 95%	18
22	May 23, 2002	LNAV/VNAV 95%	92
23	Aug 23, 2002	Chi^2 (Fig 4)	Expected high
24	Sept 4, 2002	LPV 95%	75
25	Sept 7-8, 2002	LPV 95%	0,0
26	Sept 11, 2002	LPV 95%	95
27	Oct 1-2, 2002	Chi^2 (Fig 4)	Expected low
28	Oct 4, 2002	Chi^2 (Fig 4)	Expected low
29	Nov 21, 2002	Chi^2 (Fig 4)	Expected low
30	May 29-31, 2003	LPV 95%	0, 0, 80
31	Jun 18, 2003	LPV 95%	96
32	Jul 12, 2003	LPV 95%	95
33	Oct 28-31, 2003	LPV 95%	96, 0, 0, 0
34	Nov 20-22, 2003	LPV 95%	0, 55, 72

For each epoch, a measurement of equivalent vertical delay for each WRS-to-satellite line of sight and the latitude and longitude of the ionospheric pierce point (IPP) assuming a thin shell model at 350 km altitude is included. To obtain supertruth, the raw carrier phase ionospheric delay measurements from each of the three receivers at a single WRS are leveled to the code. Then the measurements of each receiver are checked against those of the other two receivers at the same station for agreement within tight bounds. This voting process results in supertruth data, a bias- and receiver artifact-free set of ionospheric delay measurements.

Supertruth data has been generated in post-process by WAAS prime contractor Raytheon for the dates listed in Table 1. For many of the dates, low LPV service availability was observed (or expected, prior to commissioning). For some days LPV coverage was not reported by the FAA, but coverage for another level of service known as LNAV/VNAV with less stringent integrity requirements was reported. In these cases the LNAV/VNAV coverage percentage provides an upper bound to what LPV coverage would have been.

For each of the days listed in Table 1 we simulate the real-time WAAS calculation of IGP corrections and function of the Irregularity Detector, as described in detail by Walter et al [6]. IGPs are defined at regular 5x5 degree latitude and longitude intervals over CONUS. At each IGP, the IPP measurements within at least an 800 km radius but no more than a 2100 km radius are used, provided there are at least 30 of them. If, after the search radius has been expanded to 2100 km and there are fewer than 10 points, the estimate is not formed and the WAAS broadcast for that grid point is "Not Monitored." For an IGP with a sufficient number of nearby samples N, the measurements form vector $\mathbf{I_{v,IPP}}$:

$$I_{v,IPP} = \begin{bmatrix} I_{v,IPP_1} \\ I_{v,IPP_2} \\ \vdots \\ I_{v,IPP_N} \end{bmatrix} \qquad \textbf{Equation 1}$$

In the real-time system a least-squares planar fit is performed on these measurements and the resulting coefficients are used to estimate the vertical ionosphere at the IGP. For our purposes the estimate itself is unnecessary. However, the observation matrix **G**, weighting matrix **W**, and IPP measurements $\mathbf{I_{v,IPP}}$ used to perform the estimate are also used to compute chi^2. The definition of the matrices **G** and $\mathbf{W^{-1}}$ for this computation from [6] are reproduced as Equations 2 and 3 below:

$$G = \begin{bmatrix} 1 & d_{IPP_1,IGP} \cdot \hat{E} & d_{IPP_1,IGP} \cdot \hat{N} \\ 1 & d_{IPP_2,IGP} \cdot \hat{E} & d_{IPP_2,IGP} \cdot \hat{N} \\ \vdots & \vdots & \vdots \\ 1 & d_{IPP_N,IGP} \cdot \hat{E} & d_{IPP_N,IGP} \cdot \hat{N} \end{bmatrix} \qquad \textbf{Equation 2}$$

$$W^{-1} = \begin{bmatrix} \sigma^2_{I_v,IPP_1} + \sigma^2_{decorr} & \sigma_{bias,1,2} & \cdots & \sigma_{bias,1,N} \\ \sigma_{bias,1,2} & \sigma^2_{I_v,IPP_2} + \sigma^2_{decorr} & \cdots & \sigma_{bias,2,N} \\ \vdots & \vdots & \ddots & \vdots \\ \sigma_{bias,1,N} & \sigma_{bias,2,N} & \cdots & \sigma^2_{I_v,IPP_1} + \sigma^2_{decorr} \end{bmatrix}$$

Equation 3

In the weighting matrix, $\sigma^2_{I_v,IPP_i}$ is the variance that bounds receiver noise, multipath, and bias uncertainty for the i[th] IPP. The off-diagonal elements $\sigma_{bias,i,j}$ are the cross-correlations biases, nonzero if i and j share a common satellite or a common receiver. The nominal decorrelation rate of the ionosphere over CONUS is $\sigma_{decorr} = 0.35\ cm$. The chi^2 statistic is then computed as:

$$\chi^2 = I^T_{v,IPP} \cdot W \cdot \{I - G^T \cdot (G \cdot W \cdot G^T)^{-1} \cdot G \cdot W\} \cdot I_{v,IPP}$$

Equation 4

The number of degrees of freedom N_{dof} of the chi^2 statistic is the number of measurements minus the number of degrees of freedom of the model (3 for a planar fit) as given in Equation 5. The chi^2 threshold value can then be looked up in the table given in [6]; it is a function of N_{dof}. If the ratio of chi^2 to the threshold value, (Equation 7) exceeds 1, then the IGP is considered to be in a storm state and is flagged, "Do Not Use."

$$N_{dof} = N - 3$$ **Equation 5**

$$\chi^2_{thresh} = f(N_{dof})$$ **Equation 6**

$$\chi^2_{ratio} = \frac{\chi^2}{\chi^2_{thresh}}$$ **Equation 7**

Although the chi^2 ratio is slightly computationally costly, it yields a wealth of detailed spatial and temporal information that the daily LPV 95% coverage cannot, as illustrated in Figure 3. This figure compares LPV 95% coverage over time against chi2 for the extreme ionospheric storms that occurred in October and then November, 2003. The single daily LPV 95% coverage value has been assigned to the entire duration of each day. In contrast, the chi-squared ratio for every IGP has been computed every 20 minutes. Then the mean chi^2 ratio at each of three IGP longitudes – 80 W, 95 W, and 110 W - has been plotted at each epoch.

The LPV 95% coverage is zero for October 29-31, 2003, and for November 20, 2003. This is verified by the fact that the chi^2 ratio traces for 80 W (blue dotted line), 95 W (green solid line), and 110 W (red broken line) exceed 1 for enough time on those days that no part of the country could have had LPV service for at least 95% of the time. The chi^2 ratio curves yield more detailed information though. Notice that for the Halloween storm, the curve for 95 W and 110 W reach higher values than those on the east coast at 80 W, and for the November storm, the 80 W curve reaches the highest peak and 110 W exceeds one by only a factor of 20. This indicates that, while service is reduced everywhere around CONUS, certain regions may be affected by a particular storm more severely and for longer periods of time than others.

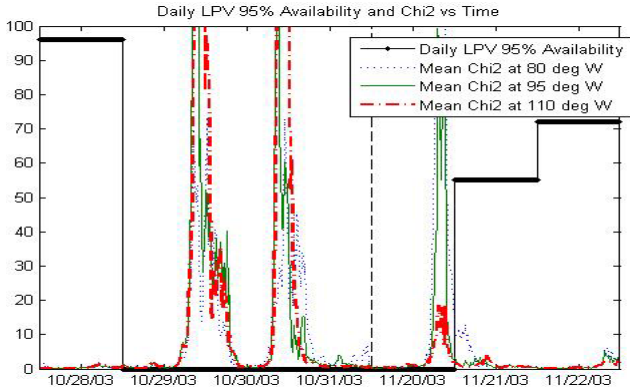

Figure 3: LPV 95% Service Coverage (thick black line), average chi-square ratio at 80 W (blue dotted line), at 95 W (green solid line), and at 110 W (red broken line) vs Time for October 2003 storm and November 2003 storm.

Chi^2 vs Kp

The geomagnetic indices Kp and Dst are publicly available online at resources such as Space Physics Interactive Data Resource (SPIDR) provided by the National Geophysical Data Center (NGDC) of the National Oceanic and Atmospheric Administration (NOAA). In this section we compare chi^2, which was shown above to be representative of availability, against the tri-hourly Kp indices for the dates listed in Table 1.

Figure 4 is a log plot of Kp (solid blue line) and of the chi^2 ratio computed every 40 minutes averaged over CONUS and over each three-hour period during each of the storms (black solid line with dots). The storm data sets are separated by vertical dotted lines and numbered according to Table 1; Kp and chi^2 are discontinuous at these date discontinuities. The horizontal red line at $\chi^2_{ratio} = 1$ marks the storm-state threshold.

The salient features of this plot are that, in general, chi^2 is high when Kp is between 7 and 9, and that chi^2 often peaks after Kp reaches its peak. This indicates that there will be some correlation, but that the cross-correlation might peak at a lag of three or six hours. Removing 0, 3, and 6-hour lags in chi^2, we find the correlation between chi^2 ratio and Kp are, 0.35, 0.40, and

0.35, respectively. These values are consistent with our observation of lag in Figure 4.

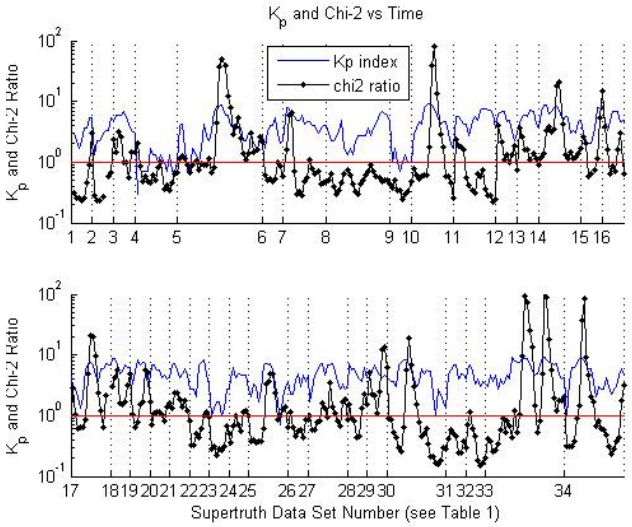

Figure 4: Kp vs time and chi^2 averaged over CONUS and over three hours vs time.

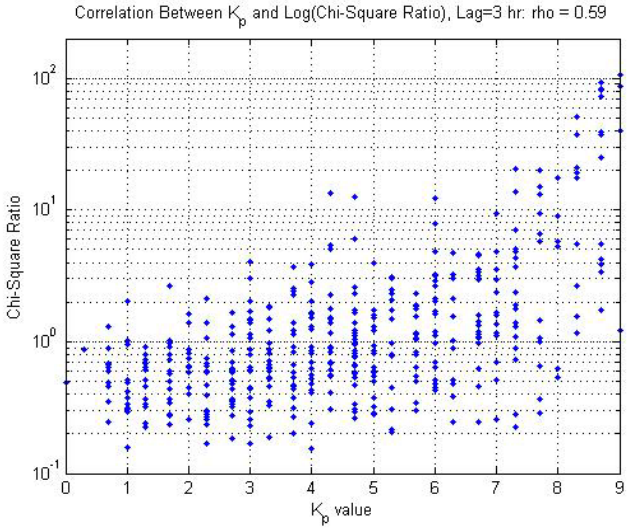

Figure 5: Log scatter plot of chi-square ratio vs Kp with chi-square ratio shifted by 3 hours.

Since the cross-correlation is a maximum for a 3-hour lag, Kp vs chi-square removing this lag is shown on a log scale scatter plot in Figure 5. Kp is quantized in thirds and shows moderate correlation of 0.40 with chi^2, but a slightly stronger correlation of 0.59 with $\log(\chi^2_{ratio})$. False alarms occur when Kp is above some specified threshold and chi-square is less than 1; this corresponds to the lower right region of the plot. If we set our threshold at Kp = 8, there are two cases where Kp = 8 and yet $\chi^2_{ratio} < 1$. Notice also that there are instances of $\chi^2_{ratio} > 1$ at nearly all values of Kp, even as low as 0.67 (often referred to as "1-"). This indicates that the cost of detecting nearly all low availability days would be to set a Kp threshold so low as to yield a great number of false alarms.

Chi^2 vs Dst

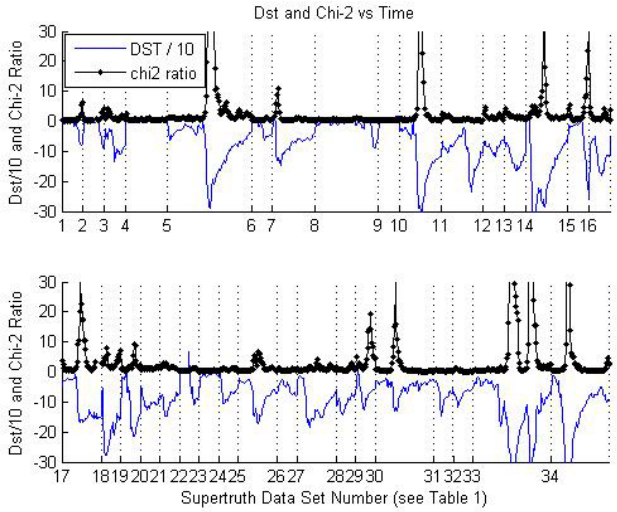

Figure 6: Dst/10 (blue solid line) and chi-squared ratio (black line with dots) vs time for each storm, numbered according to data sets in Table 1.

As an alternative to Kp, we consider the relationship between Dst and chi^2. The plot of Dst and chi^2 versus time for each storm is given in Figure 6. Dst is shown as a blue line and has been scaled by a factor of 10 for easier viewing. The chi^2 ratio is plotted as a black line with black circles at each point. Dst and chi^2 seem to spike at about the same time, and indeed, the computation of correlation coefficient for 0, 1, and 2 hour lag in chi^2 confirms this; the correlation values are -0.56, -0.53, and -0.47, respectively. As with Kp, a conversion to $\log(\chi^2_{ratio})$ produces an even stronger correlation. With no lag, the correlation between Dst and $\log(\chi^2_{ratio})$ is -0.69.

The log scatter plot of Dst vs chi-square is shown in Figure 7. Dst is an hourly value, so this figure is much more populated than Figure 5 was for the tri-hourly Kp. The false alarm region on Figure 7 falls in the lower left region of the plot. Notice that by choosing a threshold of Dst = -250 nT, we would have no false alarms with the limited number of days for which we have supertruth data, although there would be some missed detections, which correspond to the upper right region of the plot.

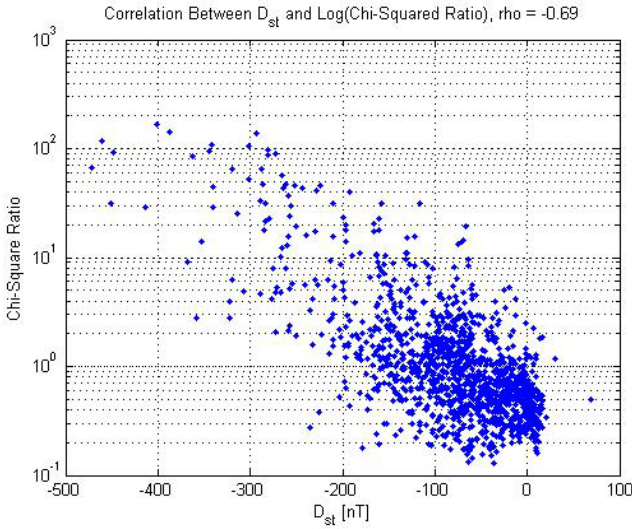

Figure 7: Log scatter plot of chi-square ratio vs Dst.

To tabulate the number of false alarms and missed detections for Kp and Dst, we return to the LPV 95% coverage numbers from July 31, 2003, through March 1, 2005, shown in Figure 1. There are a total of 610 days within this interval. False alarms occur when Dst exceeds a chosen threshold but the day is not a storm day. Missed detections are events for which Dst does not exceed the threshold, but the day is in fact a storm day. We no longer have chi-square ratio information and thus do not have the threshold of 1 at our disposal as a definition of a stormy day. For the purposes of this exercise we choose to declare a stormy day as one for which LPV 95% coverage is less than 75%. Out of the 610 days in this set, 15 are stormy, i.e. have an LPV 95% of less than 75% that is not due to other identifiable causes (such as the GEO outages mentioned above).

Missed detection rates and false alarm rates as a function of -Dst threshold (upper plot) and as a function of Kp threshold (lower plot) can be seen in Figure 8. On each of these plots the probability of missed detection P_{MD} is shown on the curve with red stars and the probability of false alarm P_{FA} is shown on the curve with green circles. The threshold is a parameter that can be tuned to achieve a desirable P_{MD} (P_{FA}) that then incurs a certain P_{FA} (P_{MD}) cost.

For the Dst threshold of -250 nT discussed above with regard to Figure 7, we find that the probability of false alarm, $P_{FA,\ Dst}$ = 1/595 = 0.17%. The single false alarm occurs for November 10, 2004, when min(Dst) = -289 nT but LPV 95% coverage = 96%. To mostly nearly meet the same false alarm rate with Kp, the threshold must be Kp = 9, the maximum possible value. There are no days for which Kp = 9 and yet coverage > 75%, so $P_{FA,\ Kpt}$ = 0/595 = 0%. With this threshold, Kp yields a missed detection rate of $P_{MD,Kp}$ = 13/15 = 87%. This is higher than the equivalent missed detection rate for Dst, $P_{MD,Dst}$ = 9/15 = 60%.

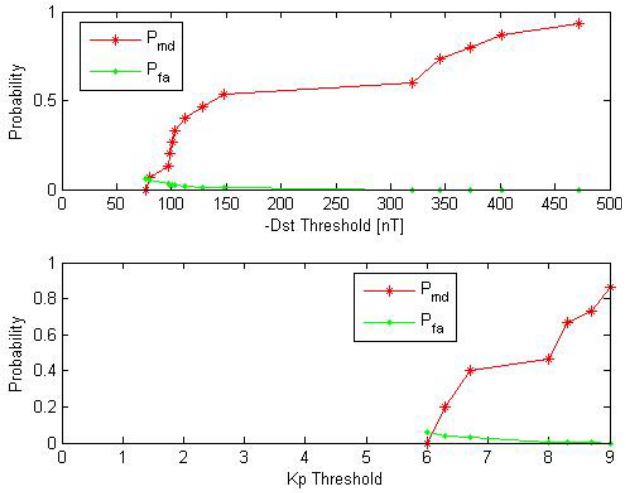

Figure 8: Probability of missed detection (red star) and of false alarm (green circle) as a function of Dst threshold (upper plot), and Kp threshold (lower plot). Based on data from 7/1/03-3/1/05.

To adjust the Dst threshold such that there are no storms that escape detection, we set the threshold to the storm day whose extreme value is least negative. Tuning this threshold is driven by March 10, 2004, which had 66% LPV coverage but minimum Dst of -77 nT. The false alarm rate for the lowest threshold that successfully detects all the storm days is then $P_{FA,\ Dst}$ = 36/595 = 6.1%. To achieve $P_{MD,Kp}$ = 0, the threshold is determined by the lowest Kp in the set of storms: 6. This yields a very similar false alarm rate to Dst: $P_{FA,Kp}$ = 37/595 = 6.2%.

We again extend the data set back to 1 Jan, 2000, and compute rates for half the solar cycle including solar maximum by relying on chi^2 as a proxy for availability. In the period between January 1, 2000, and March 1, 2005, there are over 1850 days. Of these, 47 have been identified as storms, either based on the LPV coverage percentage or on chi^2 availability (see Table 1). With this larger data set, the probabilities of missed detection and false alarm as a function of threshold are summarized in Figure 9. The upper plot shows P_{MD} (red stars) and P_{FA} (green circles) versus –Dst threshold, and the lower plot shows the curves versus Kp.

The upper plots (Dst) of Figure 8 and Figure 9 are very similar. A $P_{MD,Dst}$ = 0 can be achieved at -63 nT threshold, similar to the -77 nT threshold of the smaller data set, and it yields a comparable false alarm rate of about 11%. However, the additional data alters the Kp threshold plots (lower plots of Figure 8 and Figure 9) by filling in the region from 3 <= Kp <= 6. With the larger data set, to achieve $P_{MD,\ Kp}$ = 0, the threshold must be set at 3. This is due to April 8, 2000, which was

geomagnetically quiet following major storming on April 6-7, 2000, but would have still showed enough deviations from planarity to trip the chi^2 Irregularity Detector. This is the point at which the disadvantage of Kp as a detector becomes more pronounced; the cost of achieving $P_{MD, Kp}$ = 0 is that $P_{FA, Kp}$ = 68%.

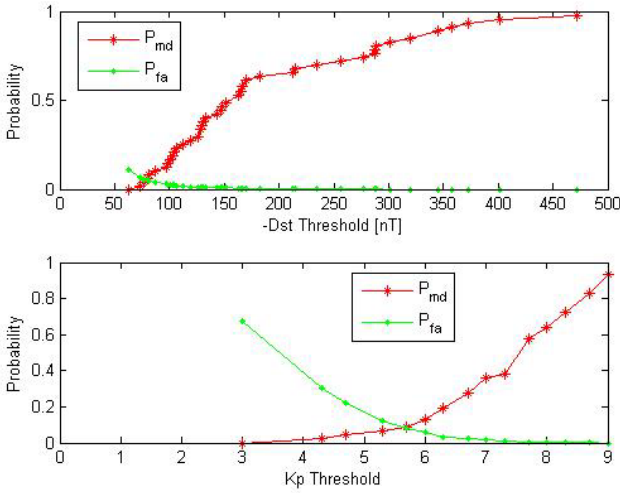

Figure 9: Probability of missed detection (red star) and of false alarm (green circle) as a function of Dst threshold (upper plot), and Kp threshold (lower plot). Based on data from 1/1/00-3/1/05.

Conclusions

This paper contrasted the use of geomagnetic index Kp with that of Dst as a predictor of WAAS LPV service coverage due to stormy ionospheric conditions. Using chi-square as a measure of availability, we find the strongest correlation of -0.69 occurs between hourly Dst and the logarithm of chi-square. The cross-correlation between Kp and log of chi-square peaks at a 3-hour time shift and is 0.59. Furthermore, by looking at 5 years of historical Kp and Dst data, we find that Dst has a lower false alarm rate than Kp for a given missed detection rate. From this information we conclude that, while Kp is a simple and handy number to generally characterize geomagnetic activity, Dst does a better job of indicating WAAS availability because chi-square tracks it slightly better. This may be due partly to the fact that Kp is averaged over three hours worldwide, whereas Dst is only averaged over an hour. Another possible explanation may be that Kp is based on measurements in the northern hemisphere that may be affected more by auroral substorm events, whereas Dst is based on equatorial measurements that show stronger sensitivity to the ring current. It is the authors' opinion that neither Dst nor Kp performs well enough to be used to forecast availability. False alarm rates on the orders of more than 10% are not acceptable for a real-time operational system. However, as a method of identifying past days that may be of ionospheric interest, Dst seems to be more reliable than Kp.

Future work will expand to include correlation of chi-squared with the regional K index, in particular K_{NA} for assessing activity in North America. This is not expected to show much improvement over Kp, primarily because it is still a tri-hourly index. Another factor identified that may show improvement over Dst alone may be the rate of change of Dst. If WAAS availability is triggered by sudden storm commencement (SSC) as the results of this paper imply, then the timing of the rate of Dst may have better performance as an indicator.

Acknowledgements

We would like to thank the FAA WAAS program for supporting this research. We would also like to thank Bill Wanner and Tom McHugh at the FAA for providing WAAS LPV availability data and the National Geophysical Data Center for making archives of geomagnetic data available at the Space Physics Interactive Data Resource.

Our thanks go out to Eric Altshuler for providing additional WAAS ionospheric data and to Michael Mendillo, Susan Skone, and several others whose helpful suggestions and feedback improved this study and provided direction for the future.

References

[1] FAA/William J Hughes Technical Center, NSTB/WAAS T&E Team, "Wide-Area Augmentation System Performance Analysis Report, Report #6," 31 Oct 2003. 14 Mar 2005. <ftp://ftp.nstb.tc.faa.gov/pub/archive/REPORTS/waaspan6.pdf>.

[2] FAA/William J Hughes Technical Center, NSTB/WAAS T&E Team, "Wide-Area Augmentation System Performance Analysis Report, Report #7," 30 Jan 2004. 14 Mar 2005. <ftp://ftp.nstb.tc.faa.gov/pub/archive/REPORTS/waaspan7.pdf>.

[3] FAA/William J Hughes Technical Center, NSTB/WAAS T&E Team, "Wide-Area Augmentation System Performance Analysis Report, Report #8," May 2004. 14 Mar 2005. <ftp://ftp.nstb.tc.faa.gov/pub/archive/REPORTS/waaspan8.pdf>.

[4] FAA/William J Hughes Technical Center, NSTB/WAAS T&E Team, "Wide-Area Augmentation System Performance Analysis Report, Report #9," Aug 2004. 14 Mar 2005. <ftp://ftp.nstb.tc.faa.gov/pub/archive/REPORTS/waaspan9.pdf>.

[5] FAA/William J Hughes Technical Center, NSTB/WAAS T&E Team, "Wide-Area Augmentation System Performance Analysis Report, Report #10," Nov 2004. 14 Mar 2005. <ftp://ftp.nstb.tc.faa.gov/pub/archive/REPORTS/waaspan10.pdf>.

[6] Walter, T., A. Hansen, J. Blanch, P. Enge, et al, "Robust Detection of Ionospheric Irregularities," Proceedings of ION GPS 2000.

[7] National Geophysical Data Center, *Space Physics Interactive Data Resource*. 1 Mar 2005. <http://spidr.ngdc.noaa.gov/spidr/>.

[8] Fares Saba, M.M., W.D. Gonzalez, A.L. Clua de Gonzalez, "Relationships between the AE, ap and Dst indices near solar minimum (1974) and at solar maximum (1979)," Annales Geophysicae 15, 1265-1270. 1997.